American Mineralogist, Volume 73, pages 1335–1345, 1988

Ostwald ripening and interparticle-diffraction effects for illite crystals

Dennis D. Eberl
U.S. Geological Survey, Federal Center, Mail Stop 404, Denver, Colorado 80225, U.S.A.
Jan Środoń
Institute of Geological Sciences, Polish Academy of Sciences, 31-002 Kraków, Senacka 3, Poland

Abstract

The Warren-Averbach method, an X-ray diffraction (XRD) method used to measure mean particle thickness and particle-thickness distribution, is used to restudy sericite from the Silverton caldera. Relative mean particle thicknesses determined by this method for the Silverton illites correlate well with cation-exchange capacity, with fixed interlayer chemistry, with an XRD intensity ratio, with the wave number of a 824–834 cm^{-1} infrared absorption band, with the Kubler index, and with the apparent K-Ar age for the samples. Apparent particle-thickness distributions indicate that the clays may have undergone Ostwald ripening and that this process has modified the K-Ar ages of the samples. The mechanism of Ostwald ripening can account for many of the features found for the hydrothermal alteration of illite.

Expandabilities measured by the XRD peak–position method for illite/smectites (I/S) from various locations are smaller than expandabilities measured by transmission electron microscopy (TEM) and by the Warren-Averbach (W-A) method. This disparity is interpreted as being related to the presence of nonswelling basal surfaces that form the ends of stacks of illite particles (short-stack effect), stacks that, according to the theory of interparticle diffraction, diffract as coherent X-ray scattering domains. Previous determinations of the charge of the illite interlayer have been based on expandability measurements that have not been corrected for the presence of these nonswelling surfaces. Thus, the value for the illite-layer charge, previously thought to be about -0.75 equivalents per $O_{10}(OH)_2$, needs revision. By using TEM methods for measuring maximum expandabilities, the fixed cation content of illite layers in I/S is determined to be approximately -0.9 equivalents per $O_{10}(OH)_2$. This charge is independent of illite origin and expandability. Based on a long extrapolation, the mean charge on exposed basal surfaces of illite particles from the Silverton caldera is approximately -0.48 equivalents per $O_{10}(OH)_2$.

Introduction

In a recent paper, Eberl et al. (1987) discussed the mineralogy of sericite from the Silverton caldera (Colorado) in terms of the theory of interparticle diffraction (Nadeau et al., 1984a, 1984b). This paper was, in part, a search to find a superior technique for studying this commonly occurring material. In the present paper, the Warren-Averbach method (Warren and Averbach, 1950) is used to measure illite-particle thicknesses with greater precision than was possible in the previous work. The better correlations found using these measurements, together with additional TEM thickness measurements of other illites, extend our knowledge of the relations between structure and chemistry for these and similar clays. In addition, apparent particle-thickness distributions suggest a mechanism for the formation and evolution of illites in hydrothermal systems.

Application of the Warren-Averbach technique

The Warren-Averbach X-ray diffraction technique was developed originally for the investigation of cold-work distortion of metals. This technique has been used by metallurgists for more than 35 years, and, in the words of Klug and Alexander (1974), "A vast amount of experience . . . supports the pre-eminence of the Fourier method of Warren and Averbach in this field." The Warren-Averbach (W-A) method separates the effects of X-ray diffraction (XRD) peak broadening related to particle size (or X-ray scattering-domain size), which is not a function of two-theta angle, from peak broadening related to strain in the crystal structure, an effect that is angular dependent, by analyzing diffraction profiles for two or more 00*l* peaks.

The present approach, which is empirical, assumes that

0003–004X/88/1112–1335$02.00

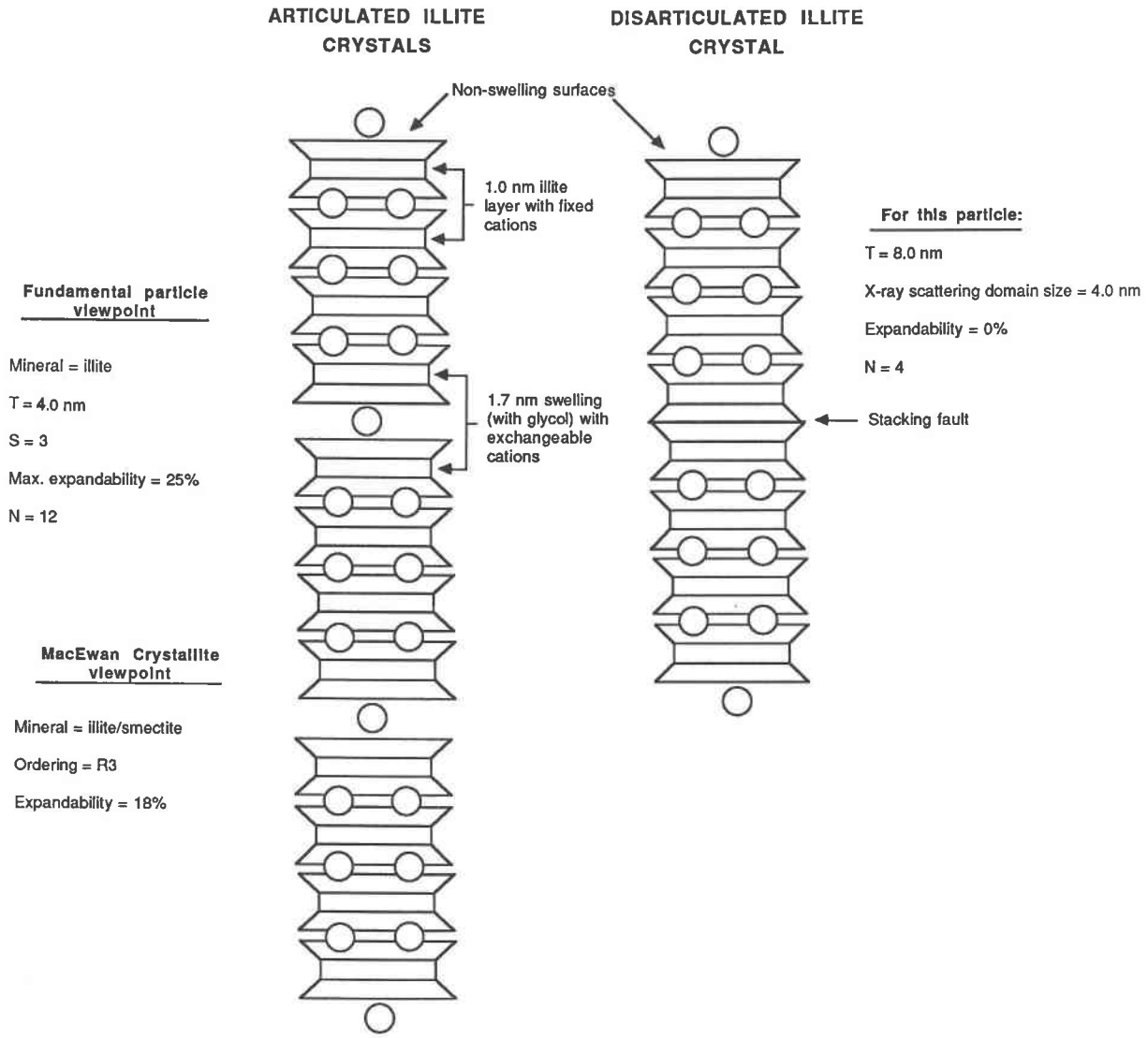

Fig. 1. A diagram that compares the fundamental-particle concept with the MacEwan crystallite concept of I/S and that presents other concepts discussed in the text. The c^* axis is parallel to the stacks. The crystallographic origin for the stacking fault is strictly speculative.

particle-size XRD peak broadening for illite is related to fundamental-particle thicknesses and that, typically, this broadening is influenced minimally by stacking faults within particles that would tend to give a smaller X-ray scattering-domain thickness than the fundamental-particle thickness. A hypothetical example of a stacking fault is diagrammed on the right side of Figure 1: the illite fundamental-particle thickness in this figure is 8 nm, whereas the X-ray scattering-domain thickness is approximately 4 nm. The interiors of the particles are assumed to be strain-free. Strain broadening for basal XRD reflections is assumed to arise entirely from interparticle swelling (the 1.7-nm spacings in the left side of Fig. 1). This "strain" is kept constant at about 1.7 nm by Sr saturation and glycolation.

The assumption that most of the particle interiors are fault-free is supported for the Silverton sericites by the data of Eberl and Velde (in prep.). This technique, which plots an XRD intensity ratio (Środoń, 1984) versus the Kubler index (Kisch, 1983), indicates that most of these sericites have XRD defect-free distances parallel to c^* that are equal to or greater than the mean particle thicknesses (defect-free distance = 20 to >40 illite layers). This technique also indicates that illites from other areas (e.g., illites from the Niger Delta basin) have defect-free distances that are less than particle thicknesses (defect-free distance 5 to 10 illite layers), in which case the W-A technique may give spuriously small mean particle thicknesses.

The assumption of strain-free interiors seems reason-

TABLE 1. Mean particle thickness (in nm) parallel to c^* measured for the Silverton sericites by the Warren-Averbach and TEM methods

Sericite	Warren-Averbach		TEM	
	Raw	Smoothed	Arithmetic mean	Weighted mean
AR1	60	18.6	—	—
AR1R	19	—	—	—
LF7	14	—	—	—
LF10	13	4.4	—	—
RM3	23	—	19	—
RM4	15	—	—	—
RM5	12	3.7	—	—
RM6	12	—	—	—
RM8	11	4.1	—	—
RM11	11	—	—	—
RM12	12	—	—	—
RM13	11	—	8	—
RM21	11	—	—	—
RM22	10	—	—	—
RM28	15	7.4	—	—
RM30	14	7.5	11	8
RM31	17	—	—	—
RM35A	11	4.1	—	—
RM35C	12	—	—	—
RM35D	12	1.6	—	—
SG1	65	13.5	—	—
SG4	29	20.0	43	28

able in applying the W-A method to sericite, because any deviation in lattice spacing (from the previously measured value of 9.99 Å) that is associated with strain within particles would be negligible compared with the large "strain" related to swelling between particles. The assumption that strain broadening is equivalent to swelling between particles—and, therefore, that its effect on XRD peak breadth can be removed for crystallite-size analysis by the W-A method—is supported by correlations that follow.

Weighted mean particle thicknesses for samples (Sr-saturated, glycolated, <2-μm size fractions) that were studied previously by other methods (Eberl et al., 1987) were determined by the W-A method from the same XRD patterns used previously (Table 1, column labeled "raw"). This analysis used the 002 and 005 XRD reflections, National Bureau of Standards standard reference material 675 (synthetic fluorophlogopite mica powder) as a calibration standard both for two-theta position and to remove the effects of machine broadening, and a Siemens-Allis[1] automated D-500 diffraction system equipped with a Diffrac V/R S software program named CRYSIZ that automatically performs the W-A analysis. In addition, weighted mean particle thicknesses (Table 1, column labeled "smoothed") and particle-thickness distributions were determined for selected samples using Siemens Diffract 500 software from additional XRD data that had been smoothed prior to Fourier analysis by using a Split-Pearson function.

[1] The use of brand names is for identification purposes only and does not constitute endorsement by the U.S. Geological Survey.

TABLE 2. Mean particle thickness parallel to c^* for sericite sample RM22 as a function of interparticle chemistry

Interparticle chemistry	Thickness (nm)
Sr-saturated, glycolated	10
Ca-saturated, glycolated	11
Mg-saturated, glycolated	11
Na-saturated, glycolated	10
K-saturated, glycolated	15
Natural, glycolated	13
Sr-saturated, air-dried	13
Ca-saturated, air-dried	20
Mg-saturated, air-dried	16
Na-saturated, air-dried	9
K-saturated, air-dried	12
Natural, air-dried	8

Note: Measurements were made by the Warren-Averbach method.

Comparisons between mean particle thicknesses measured by the XRD W-A method (raw data) and by the TEM Pt-shadowing method (Table 1, column labeled "arithmetic mean") indicate that the methods are comparable for three samples, although the W-A method generally gives greater thicknesses. However, it would be more correct to use the weighted means rather than arithmetic means as a measure of mean thicknesses. TEM particle-thickness distributions needed for this calculation were available for only two samples (Table 1, column labeled "weighted mean"). Thus, because there are insufficient TEM thickness measurements to calibrate the W-A thickness measurements, mean thicknesses and particle-thickness distributions determined by the W-A method are considered to be correct in a relative sense only, although there is some evidence from cation-exchange-capacity measurements that the mean thicknesses may be correct in an absolute sense, as will be discussed. Particle-thickness distributions calculated from the raw data, rather than from the smoothed data (Table 1), were used in subsequent analyses because the raw data set is more complete.

During application of the W-A method, it is important that the thickness of interparticle expanding layers be uniform (i.e., constant "strain"). The effect of changing the interparticle chemistry on measured particle thicknesses for a sericite sample is shown in Table 2. Air-dry sericites may contain swelling layers of different thicknesses (one or more water layers in the swelling complexes), and glycolated samples that have exchange cations of low hydration energy (e.g., K^+) also may contain two types of swelling layers (1.4 and 1.7 nm), as well as layers that have collapsed reversibly around the cation. Measurements have indicated that the interparticle Sr-glycol complex yields uniform swelling (Eberl et al., 1987).

Evidence that the W-A technique gives reasonable mean particle thicknesses is given by the correlations presented in Figure 2. The origin of the correlation between maximum expandability and an infrared absorption band (Fig. 2F) is not known. Similar correlations were made in a previous paper by using other, less precise methods to

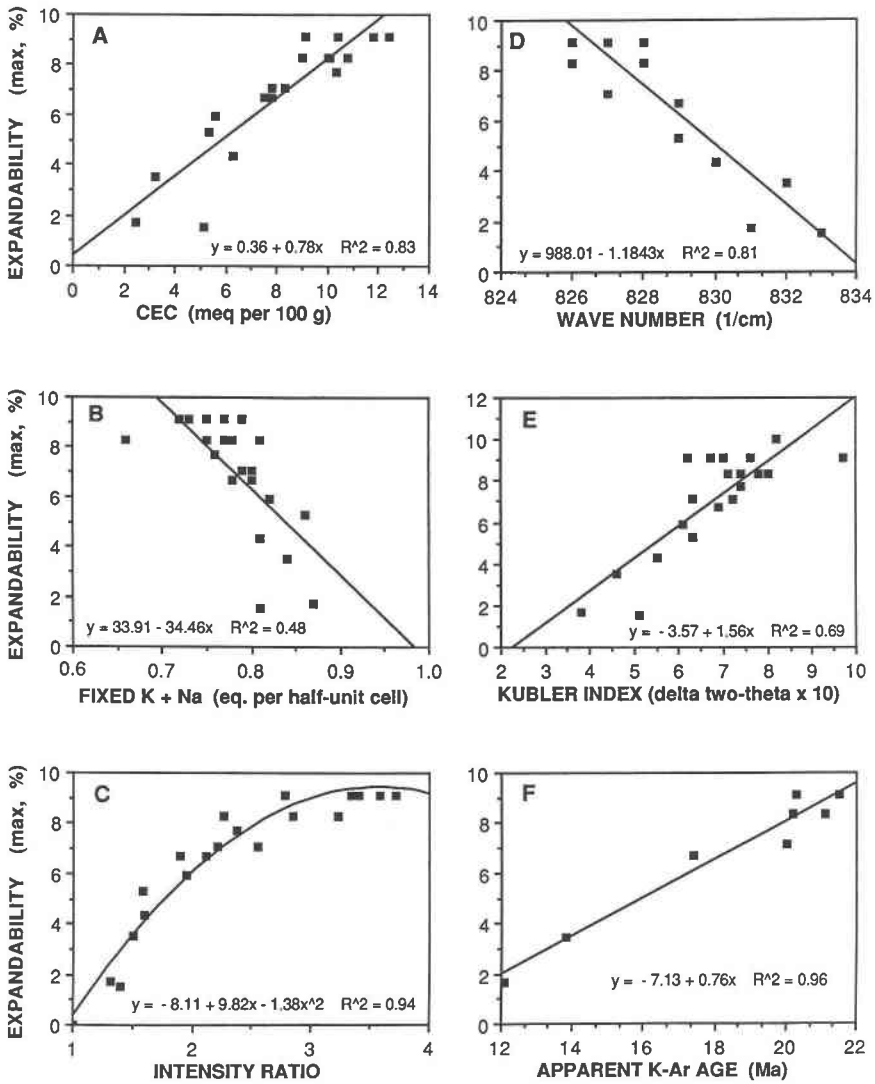

Fig. 2. Relation between maximum expandability, measured by the Warren-Averbach method, and crystal chemical properties of the Silverton sericites.

measure expandability (Eberl et al., 1987). For convenience, maximum expandability, rather than mean particle thickness, is used on the vertical axes in these figures, because maximum-expandability plots yield relations that are more linear than do particle-thickness plots. Maximum expandabilities can be calculated from mean particle-thickness measurements (T, in nm) from the equation

$$\text{Maximum expandability} = 100/T. \quad (1)$$

Maximum expandability is the expandability that would be measured if the stacks of illite particles were infinitely thick (i.e., all exposed basal surfaces of illite particles are involved in swelling), as will be discussed.

"Maximum expandabilities" rather than "expandabilities" are plotted in the figures, because expandabilities measured by the conventional XRD peak–position method depend on factors such as the thickness of the clay specimen, the arrangement of particles in the specimen, the saturating cation, and the relative humidity (Eberl et al., 1987). Expandability is a measure of how much a clay swells; as such, it would be a precise measurement, for example, in soil engineering studies where one is con-

TABLE 3. Mean particle thickness (in nm) for several sericite samples as a function of the pair of XRD reflections used in the Warren-Averbach analysis

Reflections	LF7	RM3	RM8	RM13	RM30	RM35A	SG4
001-002	12	20	2	8	12	7	24
001-003	12	20	3	8	12	7	24
001-005	13	20	3	9	12	8	25
002-003	11	17	9	9	12	7	24
002-005	14	23	11	11	14	11	29
003-005	67	38	59	—	74	1	56

cerned that clays might crack foundations. However, for understanding the problems in clay-mineral petrology (e.g., the thermodynamics and kinetics of illite formation), the mineralogically important parameters are maximum expandability, mean particle thickness, and particle-thickness distribution.

Additional evidence that mean thickness measurements given by the W-A method are precise is given in Table 3. Different combinations of 00*l* reflections were used for particle-thickness determinations for several samples. The 003-005 combination gives spurious results. All of the other combinations give good results, except for combinations containing 001 reflections for sample RM8, which is one of the most expandable samples. The 002-005 pair is the one of choice for these samples for consistent results and for avoiding the 101 quartz reflection.

In addition to mean particle-thickness measurements, the W-A method also can give particle-thickness distributions. One can be confident that the W-A method gives precise mean particle-thickness measurements for these samples, based on the good correlations given in Figure 2. In addition, extrapolation of the CEC (Fig. 2A), the intensity ratio (Fig. 2C), and the Kubler index (Fig. 2E) curves to 0% expandable gives reasonable values for nonswelling illite: a CEC of about zero, an intensity ratio of about 1.0, and a Kubler index of about 0.25° 2θ. The latter value is that cited for the anchizone-epizone boundary, at which expandability is lost (Kisch, 1983, p. 349). However, there is no direct evidence to prove that the particle-thickness distributions are correct. Confirmation of these distributions by TEM, for example, would require about a thousand particle-thickness measurements per sample (Exner and Lukas, 1971; Baronnet, 1974). (Many fewer measurements are required for *mean* thickness determinations.) Furthermore, there is at least one obvious problem with the W-A method: it is limited at the thick end of the distribution by particles that diffract as though they are infinitely thick (particles approximately >100 nm thick). These particles cannot broaden XRD peaks as a function of particle size. Also, there is a greater chance for thicker particles to be broken into coherently diffracting domains that are smaller than the fundamental-particle thickness. However, if the relative particle-thickness distributions are adopted, then the mechanism for sericite formation can be understood.

Ostwald ripening by sericite

Mean particle thicknesses determined by the W-A method reveal a linear relation between apparent K-Ar age and maximum expandability (Fig. 2F). In accordance with the available mineralogic and stable-isotope evidence (Eberl et al., 1987), two mechanisms could explain this relation. The first mechanism is mixing of clay formed during the older (22 Ma), cooler (180 °C) hydrothermal event with clay that nucleated during the younger (12 Ma), hotter (320 °C) hydrothermal event. Such an origin should lead to bimodal particle-size distributions. The second mechanism is progressive recrystallization by Ostwald ripening of the older clay during the younger event. Particle-thickness distributions indicate that the relation in Figure 2F, which could be discussed only qualtitatively in the previous paper (Eberl et al., 1987), most likely results from progressive recrystallization by Ostwald ripening (Ostwald, 1900), with a resulting partial loss of radiogenic Ar and a progressive increase in particle thickness.

According to Baronnet (1982), Ostwald ripening is characterized by the simultaneous growth and dissolution of particles of a mineral within a single medium. After nonexplosive nucleation (i.e., nucleation that takes place over a significant length of time), a system may contain a great many crystallites of different sizes. The tendency then is to minimize surface free energy by dissolving small particles and growing large particles as matter is transferred from the former to the latter through solution. By this mechanism, the average size of the particles will increase with ripening time, and the size distribution of the particles will spread out.

Apparent particle-thickness distributions for some of the dated samples are given in Figure 3. RM8, which is the oldest sample dated, also gives the simplest thickness distribution. This distribution may represent the original particle-size distribution formed by the older hydrothermal event. As the apparent age of the clays becomes younger, the particle-thickness distributions become skewed progressively toward thicker particles, as would be expected for continued ripening of the older clays by the younger event. The correlation between mean particle thickness and apparent age (Fig. 2F) thus is a function of the extent of ripening: radiogenic Ar loss from the older clays is related to mass transfer by ripening.

Ostwald ripening can be identified, and the recrystallization mechanism can be determined, by replotting grain-size distribution histograms (Fig. 3) to a plot that uses the reduced coordinates: f/f_{max}, and r/r_{mean}, where f is the frequency of a given particle radius, f_{max} is the maximum frequency encountered, r is the particle radius, which is equal to ½ the particle thickness, and r_{mean} is the mean particle radius (Baronnet, 1982). Indirect proof that Ostwald ripening has taken place is given by a steady-state profile that is independent of ripening time and of initial grain-size distribution (Lifshitz and Slyozov, 1961; Wagner, 1961). The shape and position of the normalized distribution are indicative of the growth-controlling mechanism (Baronnet, 1982, 1984).

Such normalized particle-radius histograms for several dated sericite samples and for two other illites are presented in Figure 4. Three types of steady-state profiles were found for the Silverton sericites (Figs. 4A, 4B, and 4C), two of which are very similar. The steady-state shape of the profiles from sample to sample is indicative of Ostwald ripening in a closed system. The position of the maximum and the general shape of the distributions, however, do not fit any of the calculated profiles for var-

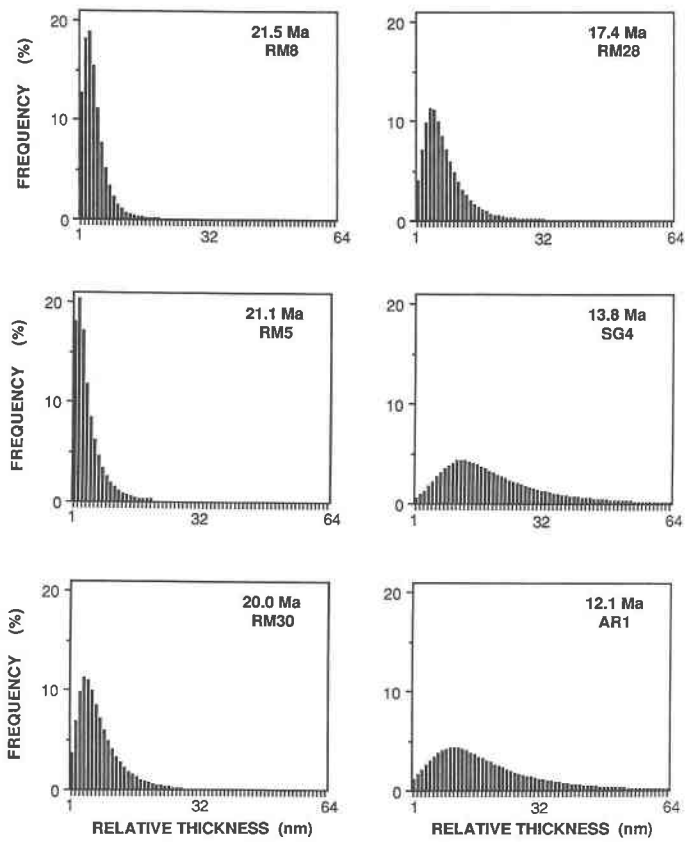

Fig. 3. Apparent particle-thickness frequency distributions for several dated samples from the Silverton caldera.

ious reaction mechanisms (Chai, 1974, 1975), some of which are presented as solid curves in Figure 4.

There are several possibilities for this lack of correlation between experiment and theory: (1) The steady-state plots in Figure 4 are artifacts of the measurement technique. This possibility seems unlikely, because several different steady-state profiles have been measured by the W-A technique. (2) The experimental plots are for rate laws that have not yet been calculated theoretically. (3) The plots actually represent cord distributions, rather than true particle-radius distributions, because the W-A method may give apparent thickness distributions that have been modified by the presence of stacking faults. A mathematical method for relating radius distributions to cord distributions has been outlined by Exner and Lukas (1971), who have made the calculation for reaction by first-order kinetics, but the calculation for second-order kinetics has not yet been attempted. It seems likely that the Silverton sericites should have reacted by a second-order rate law, because Baronnet (1974, 1982, 1984) found that the basal surfaces of phlogopite grow by second-order kinetics (spiral-growth mechanism) in hydrothermal systems. (4) Calculations for the theoretical curves (Fig. 4) are based on crystals having spherical geometry and may not be applicable to the plate geometry of clay.

The only published profile that the reduced plots for the sericites in Figures 4A and 4B come close to fitting is that measured for Fisher reagent calcite (Fig. 4D) by Chai (1975). The meaning, if any, for this apparent correlation is obscure. The reduced profiles for samples 35A and 35D (Fig. 4C) resemble those described by Baronnet (1974) for a synthetic phlogopite system for particles formed at short run times (10 min to 3 d at 600 °C and $P_{H_2O} = 1$ kbar). The distribution was interpreted by him to be transitional between a nucleation-controlled distribution and a ripening-controlled distribution (Baronnet, 1982). Samples RM35A and RM35D were collected from a broad alteration zone that was several meters wide, rather than from cracks as were the other sericites, and, therefore, they may have undergone less ripening because the plumbing was not as well developed. A very different reduced profile is given by sample MF54 (Fig. 4C), which is an illite from the central Alps (Hunziker et al., 1986).

The end of Ostwald ripening, which almost never is reached, would be the formation of one single, large crystal (Baronnet, 1984), or, more practically for clays, a number of crystals having a single, relatively large particle size. The thickest particles should record a complete history of the recrystallization, because they never have undergone dissolution. They should be zoned from an older core to a younger rim, and this zonation should be repeated going from the thinnest, oldest particles to thick-

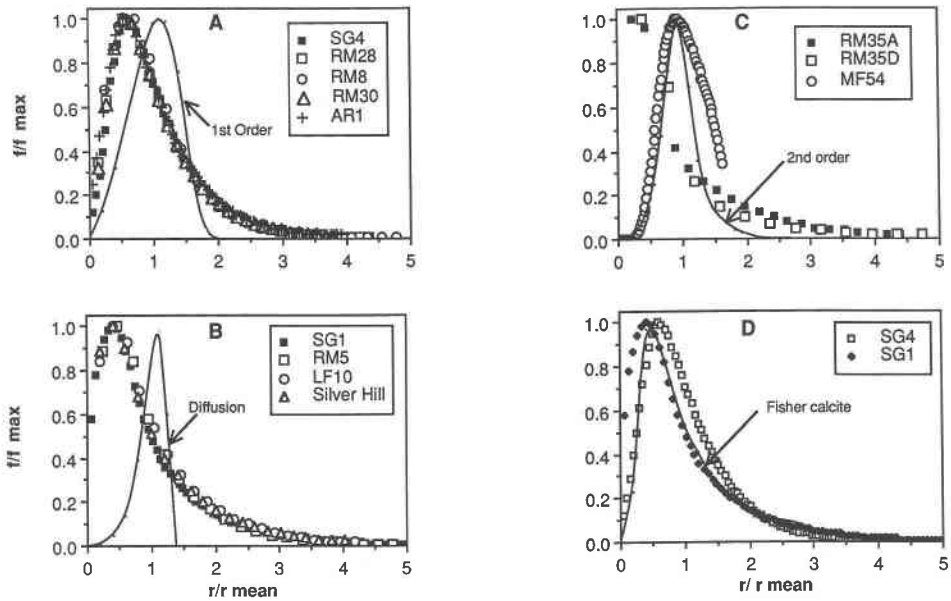

Fig. 4. Normalized apparent particle-radius histograms for K-Ar–dated sericite samples from the Silverton caldera, for the Silver Hill illite, and for an illite from the central Alps (MF54). The solid curves in A, B, and C are theoretical profiles expected for Ostwald ripening by various reaction mechanisms. The solid curve in D is an experimental curve for Fisher reagent calcite (see Chai, 1975).

er, younger particles, provided that the blocking temperature for Ar loss has not been exceeded.

Disarticulated illite particles and short stacks

The presence of disarticulated illite particles was hypothesized in the original paper (Eberl et al., 1987) in order to reconcile expandability measurements made by the conventional XRD peak–position method with those made by TEM. Expandabilities that were calculated by Equation 1 from TEM particle-thickness measurements generally were larger than those measured by XRD. The problem is presented again in Figure 5, where W-A, rather than TEM, particle-thickness measurements are used. Disarticulated illite particles do not swell (Fig. 1). Therefore, they cause the "I/S" XRD peak to migrate to a two-theta position that represents smaller expandabilities than those calculated from Equation 1, an equation that assumes that all basal surfaces are involved in swelling.

If the concept of disarticulated illite particles is valid, then this effect should influence the XRD patterns of all mixed-layer clays. Figure 6A is a plot of expandability versus fixed-cation content for I/S from a variety of environments and ages. Maximum expandabilities for the upper curve in Figure 6A were determined by TEM and Equation 1. Expandabilities for the lower curve were measured by the peak–position method of Środoń (1980, 1984). In a previous paper, the XRD curve was thought to be composed of two straight lines and to offer evidence for the existence of two types of illite layers in I/S (Środoń et al., 1986); but with the additional TEM evidence, it now seems likely that the lower position of the XRD curve is an artifact of the expandability measurement, an artifact that is related to the arrangement of illite fundamental particles on the XRD slide.

Using the NEWMOD program of R. C. Reynolds (Department of Earth Sciences, Dartmouth College, Hanover, New Hampshire 03755, U.S.A.), one can calculate the effects that disarticulated illite particles could have on expandability measurements. The program's MIXER option was used to add together appropriate illite and I/S compositions. To test the illitic end of the curve, 10% expandable, R3 I/S was mixed with illite composed of crystallites 8–10 layers thick (the thickness that would be expected for disarticulated illite particles in an I/S having this expandability). The patterns were added in the proportion 85% I/S + 15% illite. The resulting pattern does not show a peak for discrete illite, and the 17° two-theta

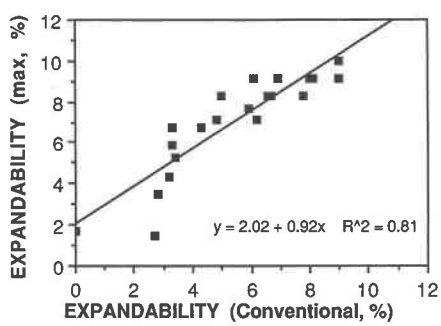

Fig. 5. Relation between maximum expandability, determined by the Warren-Averbach method and Eq. 1, and expandability determined by the XRD peak–position method.

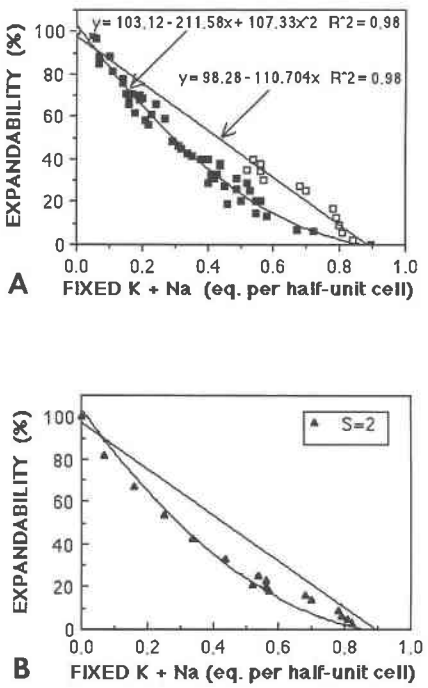

Fig. 6. (A) Relation between expandability and fixed K + Na for expandabilities measured by the TEM technique (maximum expandability calculated from weighted mean particle thicknesses, upper curve), and by the XRD peak–position method (conventional expandability, lower curve). Data for the upper curve comes from Eberl et al. (1987), Nadeau and Bain (1986), and three unpublished analyses of Silurian bentonites. Data for the lower curve comes from Środoń et al. (1986). (B) The upper curve is corrected for the effect of short stacks (stacks were assumed to contain two particles) by use of Eq. 2. The calculation shifts the upper curve, for which expandabilities were measured by TEM, downward to approximately fit the lower curve, for which expandabilities were measured by the XRD peak–position method.

reflection is displaced by an amount that is equivalent to a decrease in expandability of about 3% (see Fig. 4 in Eberl et al., 1987), which is approximately the value arrived at by deconvolution (see Table 3 in Eberl et al., 1987). Thus, disarticulation could explain the discrepancy between curves in Figure 6A for the highly illitic end.

When a similar calculation was attempted for clays having larger expandabilities, however, the discrepancy between curves (Fig. 6A) could not be reconciled. When 25% expandable, R1 I/S and discrete illite (3–5 layers thick) were added together in proportions up to 15% illite, the illite did not appear as a discrete peak, but neither did it shift the positions of the I/S peaks. On the other hand, a peak for coarse-grained illite was clearly visible in such a mixture, even if present in much smaller proportions. These calculations imply that the disarticulated-illite concept may, at best, be only a partial explanation for the discrepancy between XRD and TEM expandability measurements. The concept may apply to very illitic clays such as the Silverton sericites, but does not seem to work for R1 clays.

Thus, the concept of disarticulated illite particles needs to be modified to include the concept of "short stacks" (MacEwan crystallites). A completely disarticulated illite particle has no swelling interlayers. A stack of illite particles that contains two particles has one swelling interlayer, but two basal surfaces (one on the top and one on the bottom of the stack) that do not swell. Thus, for a given mean particle thickness, the fewer the particles in a stack, the larger the proportion of nonswelling basal surfaces, and the smaller the expandability. In a stack that contains a large number of particles, TEM expandability calculated from Equation 1 should be approached by XRD expandability measured by the peak–position method. The relation is

$$\text{XRD expandability (\%)} = 100(S - 1)/(ST - 1), \quad (2)$$

where S is the mean number of illite particles in a stack and T is the mean thickness (in nm) of the illite particles as measured by TEM. These concepts are depicted in Figure 1.

The hypothesis that the divergence of the two curves in Figure 6A is related to the presence of short stacks was tested by using Equation 2 to calculate the S required to shift the TEM line in Figure 6A to match the XRD curve. For expandabilities >40%, for which TEM thickness data are lacking, the linear-regression equation in Figure 6A was used to relate fixed-cation content to expandability, and particle thickness then was calculated from Equation 1. The calculated curve for $S = 2$ is compared with the measured curve in Figure 6B. The XRD curve can be matched exactly by assuming that S varies regularly between 1.4 for I/S of small expandability and >5 for I/S of large expandability. In other words, the thinner illite particles stack better than the thicker particles. An S less than 2 implies that the sample contains disarticulated illite particles.

If the particles are free from defects, then the mean number of coherently diffracting unit cells parallel to c^* should be $N = ST$. Thus, according to the short-stack hypothesis, a 40% expandable clay should have $N = 5$ ($T = 2.5$ from Eq. 1, and $S = 2$ from Fig. 6B), which seems small (by a factor of less than two) when compared to the N needed to model real XRD patterns of I/S (Reynolds, 1980). On the other hand, the calculated values for a 20% expandable I/S ($T = 5$, $S = 2$, $N = 10$) fall within the range required by Huff et al. (1988) to model the XRD pattern of a K-bentonite having this expandability ($12 > N > 5$) and to explain selected-area diffraction results ($T = 5$ to 10). The modeled XRD pattern of Huff et al. (1988) also required the incorporation of some segregation between illite and I/S, which may be evidence for the presence of disarticulated illite particles. A conclusive solution to the problem presented by Figure 6A probably awaits more data on the relation between particle size and X-ray scattering-domain size, and incorporation of

the interparticle-diffraction concept into Reynolds' program.

The regression equations in Figure 6A can be solved simultaneously to relate maximum expandability to expandability measured by the conventional XRD peak–position method (X). The empirical relation is

$$\text{Maximum expandability} = 55.35(0.037X + 0.041)^{1/2} - 10.87. \quad (3)$$

Mean particle thickness (T) then can be calculated from Equation 1, and mean number of particles per stack (S) can be calculated from Equation 2.

Equation 3 assumes that the relation between expandability and S varies regularly for all illite/smectites, but some clays may not fit this equation because of the effects on S of differing particle geometry, sample preparation, and crystallization history. Keeping in mind this limitation, the data of Altaner et al. (1988) can be used as an independent check of the accuracy of Equation 3 for sample RM30. These authors determined that RM30 has a maximum expandability of 22% ± 4% from a NMR inversion/recovery technique. An expandability of 6.6% measured for this sample by the XRD peak–position method (Eberl et al., 1987) yields a maximum expandability of 19% from Equation 3, a value that lies within the error range of the NMR technique. There seems to be no justification for the equation used by Altaner et al. (1988) to correct XRD expandability data for sample RM30 for the presence of MacEwan crystallites (short stacks). Even assuming that their equation is correct, using the weighted mean particle thickness for this sample as determined by TEM (Table 1), rather than the average crystallite size used by Altaner et al. (1988), their equation gives a maximum expandability of 18% (rather than 14%), close to the NMR value. Therefore, the hypothesis that this sample contains smectite sites in the interiors of illite fundamental particles is unsupported. The W-A method gives a somewhat smaller maximum expandability (14%) for this sample, and this expandability correlates well with that measured by the TEM method (13%). Clearly, more data are needed before the NMR technique for measuring maximum expandabilities can be reconciled with the other methods.

Equations 2 and 3 link the fundamental-particle concept (Nadeau et al., 1984a, 1984b) with the MacEwan crystallite concept (Reynolds, 1980; Altaner et al., 1988) of mixed-layer clays. The two models can yield different expandabilities for the same sample (Figs. 1 and 6), but both models are valid: the fundamental-particle model yields maximum expandabilities, whereas the MacEwan crystallite model yields expandabilities that are partly a function of the presence of nonswelling basal surfaces that arise from the presence of disarticulated illite particles and short stacks.

It has been puzzling that R1 ordering for I/S usually appears at about 35% expandable (e.g., Perry and Hower, 1970), because the fundamental-particle concept predicts that R1 ordering, which results from swelling between stacks of 2-nm-thick illite particles, should appear at 50% expandable I/S (Eq. 1). Likewise, R3 ordering usually appears at about 15% expandable I/S (e.g., Velde and Brusewitz, 1982), whereas the fundamental-particle concept predicts that this type of ordering, which results from swelling between particles that are 4 nm thick, should appear at 25% expandable I/S. Equation 3 may resolve this difficulty, because a 32% expandable clay (XRD peak–position method) has a maximum expandability (from Eq. 3) of 50%, and a 12% expandable clay has a maximum expandability of 28%. Na-rectorite has an expandability (XRD peak–position method) that is close to 50% and a fundamental-particle thickness that is approximately 2 nm. S must be relatively large for this situation to occur.

Charges of illite layers and particle surfaces

The precision of the present data permit calculation of the charges for illite interlayers and exposed basal surfaces. The generally accepted charge for illite layers is approximately 0.75 equivalents per $O_{10}(OH)_2$ for diagenetic clays (Hower and Mowatt, 1966; Velde and Brusewitz, 1986) and a somewhat larger value for hydrothermal clays (e.g., Eberl et al., 1987). The present approach, however, indicates that these values need revision. Based on TEM particle-thickness measurements (Fig. 6A), the best extrapolated value for the mean charge of an illite layer is about 0.9 equivalents, a value that appears to be independent of both illite origin (with the exception of illite layers formed by wetting and drying; see Eberl et al., 1986) and expandability. This fixed-interlayer-cation content is smaller than that of muscovite, and therefore illite may warrant a separate mineral name based on chemistry alone. The proposal that the illite interlayer has a larger charge than previously suspected also is supported by an extrapolation of the W-A data for the Silverton sericites (0.98 equivalents, from a correlation having a lot of scatter, Fig. 2B), by a combination of NMR and XRF data for sample RM30 (0.95 equivalents, Altaner et al., 1988, and Eberl et al., 1987), and by chemical analysis of the Kaube sericite, a nonswelling illite for which surface effects should be minimal (0.87, Środoń and Eberl, 1984).

The mean charge of the exposed basal surfaces can be estimated from an extrapolation of the curve of maximum expandability versus cation-exchange capacity (CEC, Fig. 2A), assuming that the W-A thickness measurements (raw data, Table 1) are correct in an absolute sense. Two apparently spurious CEC measurements at 22 and 24 meq/100 g have been omitted from Figure 2A. An extrapolation to zero percent expandable I/S gives a CEC of approximately zero, thereby indicating that all of the detectable CEC for the illite particles is related to basal surfaces. This extrapolation agrees with the determination of Nadeau (1987) that basal-surface area represents 95% of the total surface area of micaceous clays. The long extrapolation of the CEC versus maximum-expandability

curve to 100% expandable I/S yields a value of 128 meq/100 g for the expanding surfaces, a smectite CEC. This CEC is equivalent to a mean charge for the basal surfaces of about −0.48 equivalents per half unit cell, which is identical to the charge calculated for the surfaces of sample RM30 when the surface tetrahedral charge determined by NMR (−0.34, Altaner et al., 1988) is added to the octahedral charge determined by XRF (−0.14 from Table 8 in Eberl et al., 1987).

Conclusion

The mineralogy of sericite from the Silverton caldera can be understood in terms of the presence of illite microcrystals having various particle sizes. These crystals probably formed initially within the illite stability field, but thermodynamic equilibrium was not achieved because surface free energy was not minimized. Such a disequilibrium would lead to crystal dissolution and to crystal growth according to the theory of Ostwald ripening. The degree of ripening undergone by a particular sample most likely was a function of temperature and of time of exposure to hydrothermal fluids. These variables, in turn, may have been controlled by distance from the heat source and by plumbing. But time and temperature are not the only factors that can affect the degree of ripening.

Many of the factors that have been found to influence expandability in I/S (see Eberl et al., 1987) can be understood in terms of Ostwald ripening. For example, ripening kinetics will be enhanced by increasing temperature, by the presence of mineralizing salts that tend to increase the solubility of the clay, by increasing porosity and permeability, by stirring and flow, by fluctuations in concentrations (e.g., wetting and drying), by fluctuations in temperature, etc. (Baronnet, 1982). Conversely, crystal growth can be retarded by the presence of inhibitors.

From the viewpoint of Ostwald ripening and the theory of interparticle diffraction, it is possible to understand why the reaction of smectite to illite has proven to be difficult to reverse, why illite passes through a swelling phase as particles thicken to form nonswelling mica, and why SEM and TEM data indicate that illite both dissolves and grows in a single diagenetic or hydrothermal fluid (Pollastro, 1985; Inoue et al., 1987). However, Ostwald ripening theory is not strictly applicable to burial diagenetic sequences if the systems are open, or if other reactants are involved in the illite recrystallization process.

Conclusions drawn in this study with respect to use of the W-A method for measuring the thicknesses of swelling clays must remain tentative until this technique can be calibrated by other techniques of particle-size analysis, such as TEM. Also, although the present approach indicates that the W-A method works empirically, the W-A theory needs to be applied rigorously. The W-A method works best for clays of small expandability (<10%), whereas the XRD peak–position method is more precise for clays of larger expandability. Expandabilities measured by the latter method, however, must be corrected for the presence of short stacks if the important thermodynamic parameter of particle size is to be determined. Finally, if it is proven that a sericite (or any other clay) has reacted by Ostwald ripening, then the challenge is to separate from a single sample the various particle sizes for independent chemical, structural, and isotopic analysis. Thereby, the nucleation and recrystallization history of a sample can be determined.

Note added in proof. It has been found that the choice of a standard is crucial for determining the shape of the W-A particle-thickness distributions (Figs. 3 and 4). When a better standard was chosen (i.e., ground muscovite, which gave sharper XRD peaks than NBS 675), the reduced profiles (Fig. 4) more closely approached, although did not match exactly, the theoretical curve for reaction by second-order kinetics (spiral growth, shown in Fig. 4C). It may be that if a perfect, defect-free standard could be found and if the XRD peaks for this standard could be modeled exactly by the smoothing function, then the reduced plots for most of the Silverton sericites would match the theoretical second-order curve. Choice of standard, however, does not greatly influence mean particle-thickness measurements. We thank Myron Smith at Chevron for his help in determining the revised distributions.

Acknowledgments

Critical reviews and comments by S. Altaner, A. Baronnet, A. Inoue, P. Nadeau, R. Pollastro, R. Sanford, G. Whitney, and B. Velde are gratefully acknowledged. We thank Fred Paillet for his help with a calculation, David Bish and Steve Chipera for the use of their laboratory, and Martin Frey for supplying sample MF54. J.S. acknowledges support from The Polish Academy of Sciences Program CPBP 03.04.

References cited

Altaner, S.P., Weiss, C.A., Jr., and Kirkpatrick, R.J. (1988) Evidence from ^{29}Si NMR for the structure of mixed-layer illite/smectite clay minerals. Nature, 331, 699–702.

Baronnet, A. (1974) Étude en microscopie électronique des premiers stades de croissance d'un mica synthétique, la phlogopite hydroxylée. Phénomènes de coalescence et de murissement dans le système fermé conservatif: K_2O-6MgO-Al_2O_3-6SiO_2-excès H_2O. High Temperatures–High Pressures, 6, 675–685.

——— (1982) Ostwald ripening in solution. The case of calcite and mica. Estudios Geológicos (Madrid), 38, 185–198.

——— (1984) Growth kinetics of the silicates. A review of basic concepts. Fortschritte der Mineralogie, 62, 187–232.

Chai, B.H.T. (1974) Mass transfer of calcite during hydrothermal crystallization. In A.W. Hoffmann and B.J. Giletti, Eds., Geochemical transport and kinetics, p. 205–218. Carnegie Institution of Washington, Washington, D.C.

——— (1975) The kinetics and mass transfer of calcite during hydrothermal recrystallization process. Ph.D. thesis, Yale University, New Haven, Connecticut.

Eberl, D.D., Środoń, J., and Northrop, H.R. (1986) Potassium fixation in smectite by wetting and drying. In J.A. Davis and K.F. Hayes, Eds., Geochemical processes at mineral surfaces. American Chemical Society Symposium Series, 323, 296–326.

Eberl, D.D., Środoń, J., Lee, M., Nadeau, P.H., and Northrop, H.R. (1987) Sericite from the Silverton caldera, Colorado: Correlation among structure, composition, origin, and particle thickness. American Mineralogist, 72, 914–934.

Exner, H.E., and Lukas, H.L. (1971) The experimental verification of the

stationary Wagner-Lifshitz distribution of coarse particles. Metallography, 4, 325–338.

Hower, J., and Mowatt, T.C. (1966) The mineralogy of illites and mixed-layer illite-montmorillonites. American Mineralogist, 51, 825–854.

Huff, W.D., Whiteman, J.A., and Curtis, C.D. (1988) Investigation of a K-bentonite by X-ray powder diffraction and analytical transmission electron microscopy. Clays and Clay Minerals, 36, 83–93.

Hunziker, J.C., Frey, M., Clauer, N., Dallmeyer, R.D., Friedrichsen, H., Flehming, W., Hochstrasser, K., Roggwiler, P., and Schwander, H. (1986) The evolution of illite to muscovite: Mineralogical and isotopic data from the Glarus Alps, Switzerland. Contributions to Mineralogy and Petrology, 92, 157–180.

Inoue, A., Kohyama, N., Kitagawa, R., and Watanabe, T. (1987) Chemical and morphological evidence for the conversion of smectite to illite. Clays and Clay Minerals, 35, 111–120.

Kisch, H.J. (1983) Mineralogy and petrology of burial diagenesis (burial metamorphism) and incipient metamorphism in clastic rocks. In G. Larsen and G.V. Chilingar, Eds., Diagenesis in sediments and sedimentary rocks, Developments in Sedimentology 25B, p. 289–494. Elsevier, New York.

Klug, H.P., and Alexander, L.E. (1974) X-ray diffraction procedures for polycrystalline and amorphous materials. Wiley, New York.

Lifshitz, I.M., and Slyozov, V.V. (1961) The kinetics of precipitation from supersaturated solid solutions. Physics and Chemistry of Solids, 19, 35–50.

Nadeau, P.H. (1987) Relationships between the mean area, volume and thickness for dispersed particles of kaolinites and micaceous clays and their application to surface area and ion exchange properties. Clay Minerals, 22, 351–356.

Nadeau, P.H., and Bain, D.C. (1986) Composition of some smectites and diagenetic illitic clays and implications for their origin. Clays and Clay Minerals, 34, 455–464.

Nadeau, P.H., Wilson, M.J., McHardy, W.J., and Tait, J.M. (1984a) Interparticle diffraction: A new concept for interstratified clays. Clay Minerals, 19, 757–769.

——— (1984b) Interstratified clays as fundamental particles. Science, 225, 923–925.

Ostwald, W. (1900) Über die vermeintliche Isomerie des roten und gelben Quecksilberoxyds und die Oberflächenspannung fester Körper. Zeitschrift für Physikalische Chemie, Stöchiometrie und Verwandschaftslehre, 34, 495–503.

Perry, E., and Hower, J. (1970) Burial diagenesis in Gulf Coast pelitic sediments. Clays and Clay Minerals, 18, 165–177.

Pollastro, R.M. (1985) Mineralogical and morphological evidence for the formation of illite at the expense of illite/smectite. Clays and Clay Minerals, 33, 265–274.

Reynolds, R.C. (1980) Interstratified clay minerals. In G.W. Brindley and G. Brown, Eds., Crystal structures of clay minerals and their X-ray identification, p. 249–303. Mineralogical Society, London.

Środoń (1980) Precise identification of illite/smectite interstratifications by X-ray powder diffraction. Clays and Clay Minerals, 28, 401–411.

——— (1984) X-ray identification of illitic materials. Clays and Clay Minerals, 32, 337–349.

Środoń, J., and Eberl, D.D. (1984) Illite. Mineralogical Society of America Reviews in Mineralogy, 13, 495–544.

Środoń, J., Morgan, D.J., Eslinger, E.V., Eberl, D.D., and Karlinger, M.R. (1986) Chemistry of illite/smectite and end-member illite. Clays and Clay Minerals, 34, 368–378.

Velde, B., and Brusewitz, A.M. (1982) Metasomatic and non-metasomatic low grade metamorphism of Ordovician meta-bentonites in Sweden. Geochimica et Cosmochimica Acta, 46, 447–452.

——— (1986) Compositional variation in component layers in natural illite/smectite. Clays and Clay Minerals, 34, 651–657.

Wagner, C. (1961) Theorie der Alterung von Niederschlägen durch Umlösen (Ostwald-reifung). Zeitschrift für Elektrochemie, 65, 581–591.

Warren, B.E., and Averbach, B.L. (1950) The effect of cold-work distortion on X-ray patterns. Journal of Applied Physics, 21, 595–599.

Manuscript received March 21, 1988
Manuscript accepted July 27, 1988